Soot reduction for cleaner Compression Ignition Engines through innovative bowl templates

José V. Pastor, Antonio García, Carlos Micó, Felipe Lewiski,

[a]CMT - Motores Térmicos, Universitat Politècnica de València, Camino de Vera s/n, 46022 Valencia, Spain

Corresponding author (*): Carlos Micó

e-mail: carmirec@mot.upv.es

Phone: +34 654919619

Abstract

Considering the need of pollutant emissions reduction and the high cost of the after-treatment systems, in-cylinder solutions for pollutant reduction are becoming more and more relevant. Among different proposals, new piston geometries are considered an attractive solution for reducing both soot and nitrogen oxides emissions in compression ignition engines. For this reason, this paper evaluates the soot formation and combustion characteristics of a novel piston geometry proposal, called stepped lip-wave, for light-duty engines. It is compared with other two well-known bowl geometries: re-entrant and stepped lip. The study was performed in an optical single-cylinder direct injection compression ignition engine. Two optical techniques (2 color pyrometry and OH* chemiluminescence) were applied for analyzing soot formation in each piston geometry. Test were performed at different engine loads, fuel injection characteristics and exhaust gas recirculation configuration. The re-entrant piston presents higher soot formation and a slower late oxidation process in comparison with the other two geometries. Stepped lip and stepped lip-wave present similar soot formation levels. However, stepped lip-wave showed a more efficient and faster soot oxidation process during the final combustion stages. Results confirm the potential of the stepped lip-wave concept to reduce soot emissions and achieve a cleaner energy production system.

Keywords

Soot reduction; Innovative bowl templates; Optical engines; Optical Techniques; compression ignition.

1. Introduction

Pollutant emissions nowadays is one of the key topics in the internal combustion engines (ICE) field. The automotive industry and research centers are working hard to fulfil current and future regulations [1,2]. In general, the pollutant emission problems in ICEs can be approached by means of two ways. The first way is related with the active solutions, which prevent or reduce the pollutant formation inside the combustion chamber. The second way is based on passive solutions, where the pollutants are treated outside of combustion chamber, after the combustion process have finished. Although the after-treatment systems have allowed the ICEs reach the pollutant emissions target, the production cost of engines has increased significantly[3,4]. Besides that, the aftertreatment systems have faced difficulties with the low temperature combustion modes. In this way, the reduction of in-cylinder pollutant formation emerges as an attractive solution. Focusing on the diesel combustion, pollutant formation is a complex problem due to the soot and NO_X trade-off [5,6]. In order to meet the emissions levels required by regulations and reducing fuel consumption, different technologies regarding in-cylinder pollutant formation reduction have been tested and implemented in CI engines during the last decades[7–10]. A special attention has been paid on new piston geometries, where different designs have been developed and tested during the last years in order to study the effect of piston geometry on turbulent flow structure[11], soot formation[12] and thermal efficiency[13].

The engine-out soot emissions in CI engines depend of two main process: in-cylinder soot formation and soot oxidation. Therefore, they could be reduced by either forming less soot during the combustion process or improving the soot oxidation rate. The interaction between the spray and piston, as well as the chemical and physical properties of a specific fuel will impact directly on the local fuel/air ratios, affecting the fuel-air mixing and combustion process[14]. Studies regarding injection pressure and number of injections have shown a great potential in terms of soot reduction, due to an improvement in the fuel atomization and an increasing of turbulent mixing energy [15–17]. However, an increase of NO_X formation due to the higher flame temperatures is also reported by most of the studies [18,19]. Recent studies have shown a potential reduction of soot emission by promoting the soot oxidation during the late cycle burn out phase, when the injection event has already ended [20,21]. The efficiency of the late-cycle soot oxidation process is related with the turbulent flow field, as well as the spray-wall interaction. Both factors are conditioned by the piston bowl geometry.

Several studies regarding the in cylinder flame movement and its interaction with walls have been carried out with different piston geometries, for both high and low swirl CI engines [14,22,23]. The type of piston which is typically used in low and medium-duty engines is known as re-entrant (ω shape). A sketch is represented in Figure 1. This bowl geometry is characterized by creating a swirl supported ambient and promoting fuel-air mixing. With this geometry, once the injection plumes reach the limit of the bowl, they are directed toward the piston center and down into the bowl [20]. For low swirl ratio engines, where the tangential gas movement is weak, the piston shape is usually an open bowl [22,24,25].

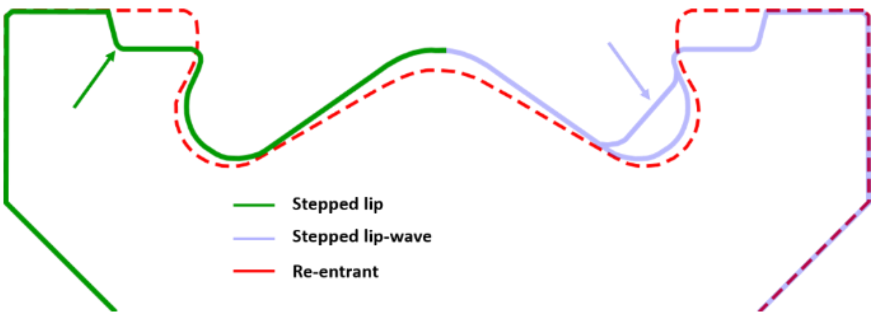

Figure 1- Sketch of the pistons used for the current study

Regarding light-duty applications (swirl-supported diesel engines), different bowl geometries, based on the re-entrant one, have been developed during the last years. One of them is the stepped lip shape. In this case, the protruding lip of the re-entrant piston is replaced by a chamfered or stepped lip as indicated by the green arrow in Figure 1. Several works have analyzed the impact of this geometry on the diffusive combustion[14,26–28]. In general, results suggest that the stepped lip improves the fuel/air mixing on the squish zone due to the split of spray into two parts. Therefore, a more complete combustion process is generated. In addition, the improvement of the mixing process leads to a reduction in combustion duration and an improvement in terms of fuel consumption. The stepped lip bowl geometry developed by Honda and named "two-stage chamber" was tested by Neely et al.[29] . Results showed an appreciable soot emissions reduction. The NO_X emissions were also reduced due to the possibility of using high EGR ratio without significant smoke increases. At high loads, an enhancement of fuel consumption was reported as well.

Another piston bowl geometry which is based on the stepped lip design was developed, tested [30] and patented [31] by Ricardo UK company in 2011. The tests of this piston geometry, called "Twin Vortex Combustion System", were performed in JCCB off-highway diesel engines. The engines met the Tier 4 interim/Stage 3B legislation without using any kind of aftertreatment [30]. In the same way, the ULPC piston (Ultra-Low Particulate Combustion) for light duty and commercial applications, based on a stepped lip design, was tested by Yoo et al.[32]. It was reported a reduction of soot emissions over 60% with an improvement in NOx-soot trade-off. The Mercedes-Benz OM654 engine, which uses a stepped lip bowl, was recently launched by the company. Benefits in terms of air utilization and low particulate emissions were reported [33].

Recently, the Volvo Group has presented a new piston geometry [34]. It has been named as “wave piston” and it has been designed for truck engines. In this piston, a kind of protrusions (waves) are located at the bowl periphery, equally spaced around the whole circumference. The corresponding profile has been represented in Figure 1, where it can be compared with the conventional stepped lip geometry. The wave protrusion is indicated by the blue arrow. The results have shown a great potential in terms of soot reduction while keeping low NO_X levels due to the efficient late cycle oxidation promoted by the bowl design [12,35]. Eismark et al.[34] tested this piston geometry in a high pressure/high temperature spray chamber and in a single cylinder engine. A strong decrease of up to 80% in soot emissions without NO_X emissions penalization were found by the authors during the tests. Soot images have shown that the wave protrusions avoid the flames to spread tangentially when they reach the bowl periphery. On the contrary, they are directed towards the piston center, where more oxygen is available. The movement contributes to improve the soot oxidation and to generate faster soot burn-out.

Although the potential of wave-protrusions has been explored for heavy-duty engines, this concept has never been applied in light-duty engines. In this way, the present work aims to fill this gap by proposing a new piston template for light-duty diesel engine applications. It combines two features that have shown interesting results in terms of soot reduction: stepped lip and wave protrusion. In order to evaluate the performance of the new proposal, a comparison is carried out with the “simple” stepped lip and reentrant geometries. In order to achieve this goal, an optical diesel engine equipped with three distinct transparent piston geometries (reentrant, stepped lip and stepped-lip-wave) was used. In order to quantify the soot generated by each bowl geometry and differences in the combustion process, two different optical techniques were applied at the same time: 2 color pyrometry (2C) and OH* chemiluminescence. A general comparison between re-entrant and hybrid piston was performed by applying a reference test condition (4.5 bar IMEP). For the comparison between stepped lip and stepped lip-wave geometries, a sweep of different IMEP, SOE, post injection and EGR at 8.9 bar IMEP were applied. These sweeps of conditions had the objective of promoting higher soot formation and evaluating the wave potential. By means of the two optical techniques applied in the current work, the differences in terms of soot formation, soot oxidation and thermodynamic characteristics were studied and discussed in the results section. The results have shown a good potential of the wave protrusions in order to diminish the soot emissions during the late combustion cycle. Taking into account the present scenario of the strict emissions regulations, this study provides an important and innovative contribution in searching new technologies for pollutant reduction and cleaner energy production.

2. Material and Methods

2.1. Optical Single Cylinder Engine

An optical single-cylinder direct injection compression ignition engine was used for this work. It is equipped with a Bowditch piston extension and is based on a GM 1.6L commercial diesel engine, as shown in Figure 2. The optical engine uses an original GM cylinder head, with 2 intake and 2 exhaust valves and a solenoid injector with 8 holes nozzle, located at the center of the cylinder. In addition, the stroke and bore are the same used in the original GM engine. The most relevant geometric parameters are summarized in Table 1.

Table 1. Optical engine characteristics

Engine characteristics	4 stroke, direct injection
Number of cylinders [-]	1
Valves [-]	4
Stroke [mm]	80.1
Bore [mm]	80
Compression ratio [-]	12.5:1(re-entrant) / 11.5:1(hybrid)
Bowl Types	Re-entrant /stepped lip/stepped lip-wave
Displacement [l]	0.402

The combustion chamber is visualized thanks to the use of a full-quartz piston top and an optical access from the piston bottom. The quartz pistons were manufactured with a bowl shape similar to the full-metal ones, to reproduce the combustion behavior and flow pattern of the corresponding metal engine. The air leakages (blow-by) is minimized by using special piston rings (synthetic material), which expands with temperature.

A DRIVVEN® control unit manages all injection system. It allows high flexibility in terms of injection settings, including the possibility of defining the number of cycles at firing conditions (skip fire mode). In addition, the system is equipped with a conventional fuel pump and common rail.

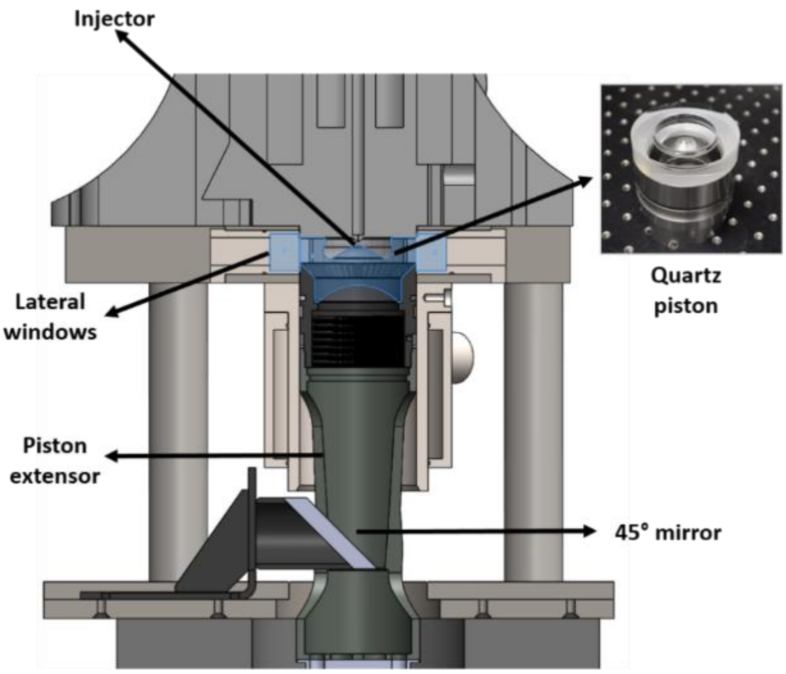

Figure 2- Optical Engine

2.2. Engine test cell

The test cell and all equipment necessary to operate the engine is represented in Figure 3. For each test condition, the intake air is supplied by a screw compressor at the required pressure. Settling chambers are installed in both intake and exhaust lines. Besides, a heat exchanger and a dryer are used for preparing the intake air before it reaches the settling chamber. An additional air heater is also located at the settling chamber with the purpose of ensuring a constant intake air temperature. A backpressure regulator is installed in the exhaust system.

An electric dynamometer is used to motorize the optical engine and control the engine speed and load at firing conditions. The instantaneous in-cylinder, intake and exhaust pressures were measured with a piezoelectric transductor (AVL GH13P) and a charge amplifier (Kistler 4603B10). A Yokogawa DL7008E oscilloscope recorded the instantaneous pressure signals, which were synchronized by a shaft encoder. Table 2 shows the accuracy of the different elements of the test cell.

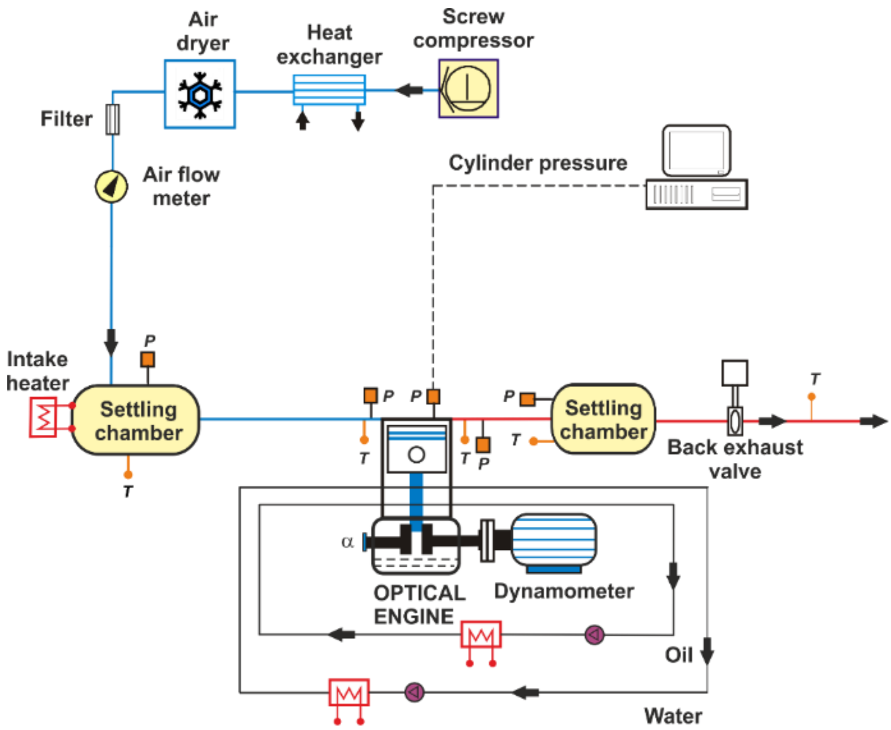

Figure 3 – Test cell diagram

Table 2 – Accuracy of the sensors

Variable	Device	Manufacturer / model	Accuracy
In-cylinder pressure	Piezoelectric transducer	AVL / GH13P	±1.25 bar
Intake/exhaust pressure	Piezorresistive transducers	Kistler / 4603B10	±25 mbar
Temperature in settling chambers and manifolds	Thermocouple	TC direct / type K	±2.5 °C
Crank angle, engine speed	Encoder	AVL / 364	±0.02 CAD
Air mass flow	Air flow meter	Sensyflow / FTM700-P	< ±1%

2.3. Bowl geometries

For the present work, three different bowl geometries are tested in the optical engine under real operating conditions. A re-entrant bowl geometry (Figure 4a), which is the most typical bowl geometry in light-duty engines, is considered as the baseline piston. The second piston is a hybrid design which contains two bowl geometries. One half of the bowl, shown in Figure 4b, contains only the stepped lip feature. The other one is composed by a merge between stepped lip and wave protrusions. The hybrid piston was manufactured in order to allow a simultaneous comparison between two geometries (stepped lip and stepped lip-wave) in terms of combustion process, soot formation and soot oxidation, reducing as much as possible the uncertainties induced by the cycle to cycle variations.

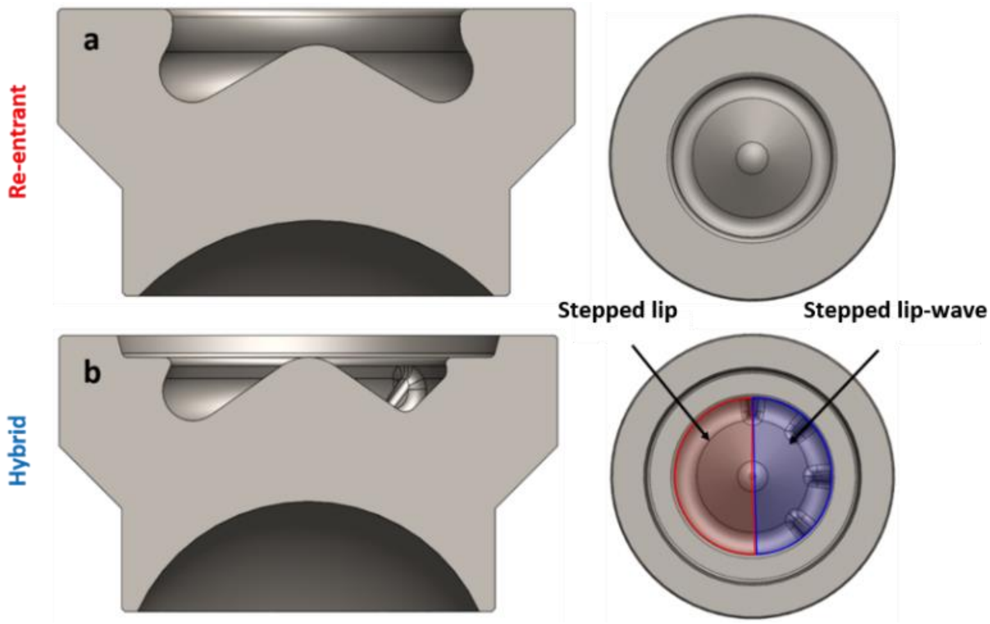

Figure 4 – Bowl geometries: a) Re-entrant. b) Hybrid

2.4. Operating conditions

For the reference case, the experiments were performed at 4.5 bar IMEP and commercial diesel was used as the fuel. A sweep of start of energizing (SOE), post injection and EGR at higher IMEP (8.5 bar) were also tested. For all operating points, the engine was kept at 1250 rpm. Table 3 is showing the test matrix with the engine operating conditions used in the current work. Taking into account that the two pistons have different compression ratio (C_r), in order to maintain the same IMEP, mass of fuel injected per cycle and maximum in-cylinder pressure were constant among geometries while different intake pressure and intake temperature were defined for each piston. The result of the intake thermodynamic adjustment between both pistons is represented in Figure 5. It was based on achieving the same P_{max} and density for motored cycles, which allows a direct comparison between both pistons. In order to simulate the exhaust back pressure, the intake pressure was set 0.2 bar lower than the exhaust pressure. The engine coolant temperature was kept between 15 °C and 25 °C for preserving the piston rings, which are made from a synthetic material.

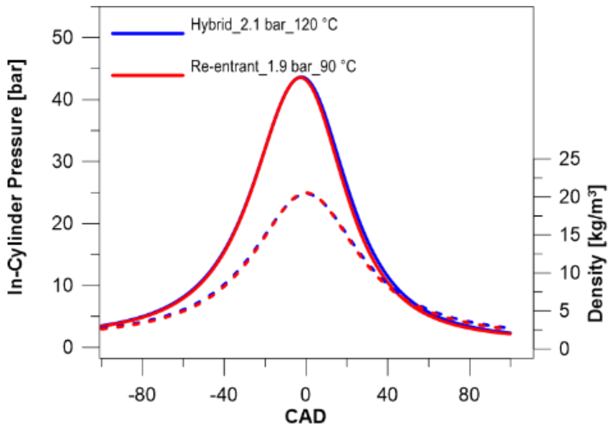

Figure 5 – motored In-cylinder pressure and density used at 4.5 bar IMEP

Table 3- Engine operating conditions

Case	Inj. Pattern	Engine Speed	Piston	IMEP (bar)	Pinj (bar)	Pint (Bar)	Tint (°C)	Toil (°C)	Tcool (°C).
Reference	Mult.	1250	Re-entrant	4.5	670	1.9	90	60	15-25
			Hybrid			2.1	120		
Sweep : SOE, Post and EGR	Mult	1250	Re-entrant	8.9	800	2.15	100	60	15-25
			Hybrid			2.4	125		

Multiple injections (pilot 1, pilot 2, main and post) were configured to reproduce a commercial injection strategy. Different injection pressures were used as shown in Table

3. The injection rate was measured in a mass flow rate device. By means of these measurements, it was obtained the total mass of fuel injected for each operating condition.

2.5. Optical Techniques

In the present work two different optical techniques were used. The optical assembly for the current work is shown in Figure 6. To measure OH* chemiluminescence, the UV radiation was reflected by a dichroic mirror and recorded with an intensified camera, which was mounted in parallel with the engine's crankshaft. This element is transparent to the visible spectrum (up to 750 nm) so light transmitted was used for 2 color pyrometry measurements. Two high speed cameras were mounted perpendicularly, each of them equipped with an interference filter, centered at 550nm and 660nm (10 FWHM) respectively. A beam splitter (50/50) was installed in order to transmit 50% of the flame radiation to one of the cameras and reflect the other 50% to the other camera.

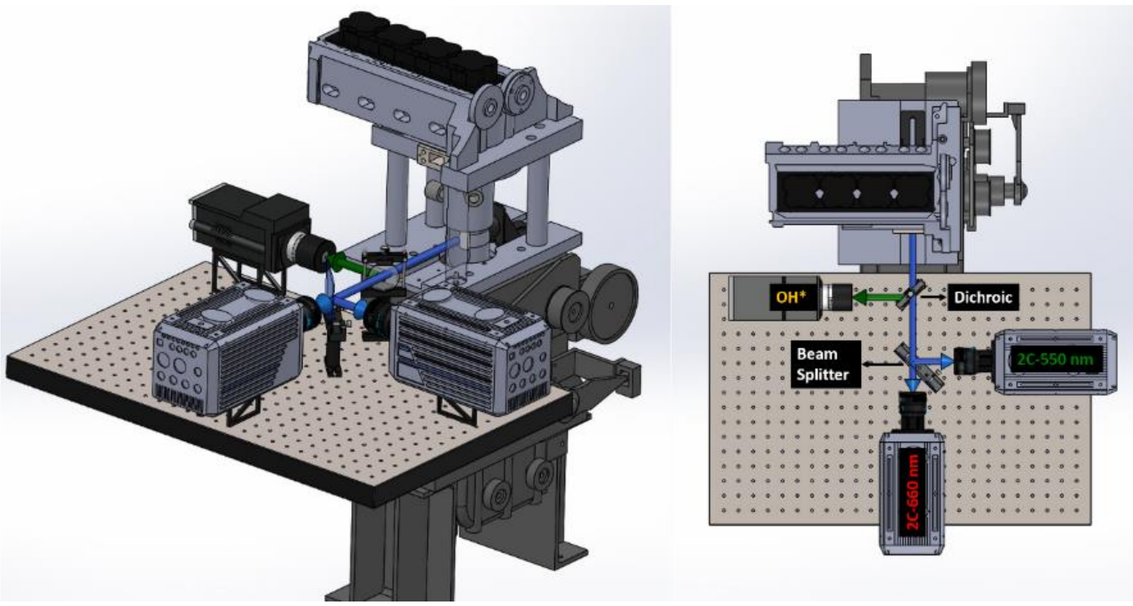

Figure 6 - Optical setup

2.5.1. OH* chemiluminescence

The high temperatures zones, where the soot oxidation is promoted, were visualized by the radiation of OH* molecules in excited state. An intensified camera (Andor Solis iStar DH334T-18H-83) with a Bernhard-Halle UV lens and a 310 nm ± 10 nm bandpass filter were used for the measurements. The spatial resolution of the images was 8.7 pixel/mm. Due to the maximum framerate of the camera, only one image per cycle was recorded. Thus, a sweep of 6 different CAD's was performed to register the time evolution of the OH*-chemiluminescence.

2.6. 2-color pyrometry

The 2-color pyrometry technique is based on measuring soot thermal radiation at two specific wavelengths. Both signals are combined to obtain the optical density and temperature of the soot surface [36]. The soot emission spectrum is represented by the Planck's law:

$$I_b(T,\lambda) = \frac{C_1}{\lambda^5 \left[e^{\left(\frac{C_2}{\lambda T}\right)} - 1 \right]} \qquad (1)$$

Where I_b is the radiance emitted by soot, $C_1 = 1.1910439\, x\, 10^{-16} Wm^2/sr$ and $C_2 = 1.4388\, X\, 10^{-2}\, mk$ are the first and second Planck's constants and λ is the wavelength. This expression considers that soot is a black body emitter. Thus, in order to consider its real emission properties (ε < 1) equation (1) is modified as follows:

$$I(T,\lambda) = \varepsilon I_b(T,\lambda) \qquad (2)$$

The emissivity can be expressed in terms of soot properties, according to the Hottel and Broughton (1932) empirical correlation[36] that is represented by equation 3:

$$\varepsilon(KL,\lambda) = 1 - e^{-\left(KL_{2C}/\lambda^{\alpha}\right)} \qquad (3)$$

Where α = 1.39 for most fuels within the visible range [36]. The soot concentration is related with the KL_{2C} parameter. It represents all the soot along the optical path of the flame, no matter either its geometrical size or distribution [37]. When radiation is measured at two different wavelengths, it is possible to calculate temperature and KL_{2C} by applying equation 2 to both of them.

In this work, two identical detection systems were used to register radiation at 550 and 660 nm. In both cases, it was used a high-speed camera (Photron SA-5) in combination with a 100mm focal length and f/2 lens. The lenses were used with a wide-open aperture. The image was focused in the region closer the quartz surface with the piston at TDC. The acquisition rate was set to 25 kfps. A different exposure time was set for each camera, in order to maximize the dynamic range used for both of them: 6.65 µs for 660 nm and 10.05 µs for 550 nm. A tungsten-ribbon calibration lamp (Osram Wi17G) was used for calibrating the detection system. The procedure followed was already applied in other studies [37,38]. The calibration lamp was located on top of the piston (flat area) and all the optical elements used in the tests were included (beam splitter, mirrors and filters).

2.7. Methodology for 2D evolution map analysis

For the image analysis it was developed a specific methodology which reproduces the KL temporal and spatial evolution in a single map. The KL images for each instant, which are the average of 6 combustion cycles, were divided in rings of different radius as shown in Figure 7. The difference between the external and internal radius for each ring is 0.5 mm. For each ring, an average KL and the mean radius are calculated. The equation 4 summarizes the average KL calculations:

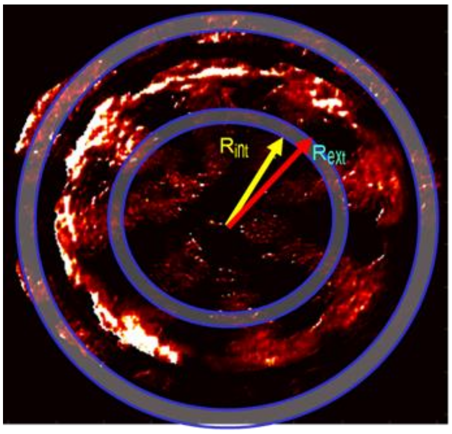

Figure 7- Rings used for the analysis

$$KL_{mean} = KL_{cummul,a}/A_a \tag{4}$$

Where the A_a is the current area or total amount of pixel present at each ring region. $KL_{cummul,a}$ is the sum of all soot pixel (KL) values contained in the ring. The mean KL value for each region is calculated from the ring area A_a and $KL_{cummul,a}$.

For the hybrid piston, an additional methodology was applied in order to isolate the two different regions, one corresponding to the stepped lip side and the other to the stepped lip-wave side. For this purpose, two sectors were defined. It was decided to separate them as much as possible and to minimize the crosstalk between both geometries. The sectors chosen to analyze stepped-lip and stepped-lip wave geometries are shown in Figure 8. The center of the bowl was excluded as it was observed that it induces high light reflections and distortions. In addition, the squish zone was also not considered for the analysis due to the difficulty of isolating the impact of the waves in this region, considering that the waves are inside the bowl. Taking this into account, for the re-entrant piston the same bowl region was considered. As the flame region considered for the analysis is located inside the piston bowl and close to the quartz surface, it was assumed that the optical distortion has not effect for the direct comparison between both pistons.

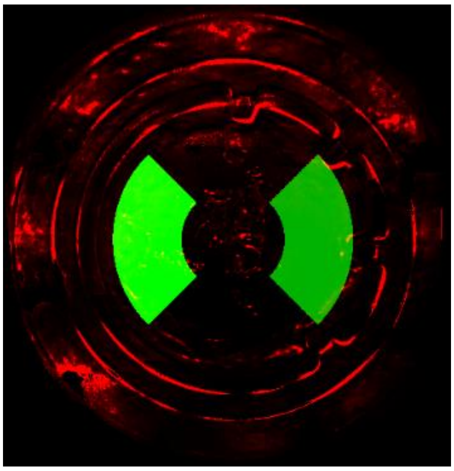

Figure 8 - Regions considered for 2D maps evolution using the hybrid piston

2.8. In-cylinder pressure analysis

The in-cylinder pressure measurements were used to calculate the rate of heat release (RoHR). The RoHR curve was calculated by means of an in-house developed tool [39,40] which is based on first law of thermodynamics. One zone model is applied for the analysis, where is considered only the time that both exhaust and intake valves are closed. In addition, blow-by, heat transfer and mechanical deformations are also considered in the model. An specific characterization was developed for this optical engine [41], which has been used also in this work.

3. Results and discussion

First, in the results section, an analysis of in cylinder pressure is presented for the reference condition (4.5 bar IMEP), as well as the sweeps of SOE, post injection and EGR at 8.9 bar IMEP for both piston geometries. Then, an analysis of OH*chemiluminescence and 2C pyrometry will be performed for the reference case, highlighting the differences between the re-entrant and hybrid piston. The second part of the results section will be focused only on the analysis of the hybrid piston, where the main differences due to the sweep of different conditions will be analyzed for stepped lip and stepped lip-wave bowl geometries.

3.1. Hybrid piston vs Re-entrant piston

The in-cylinder pressure and RoHR for the reference condition as well as for the sweeps of SOE, post injection and EGR are presented in Figures from 9 to 14. A satisfactory agreement between the in-cylinder pressure and its evolution for both pistons can be appreciated. In general, the rate of heat release of both pistons is similar. However, still some differences can be detected. For most of the cases, the hybrid piston burns the pilot 1 faster than the reentrant one, as the RoHR at this stage is higher. This effect is not visible for the case of EGR. This suggest that the air-fuel mixing promotion created by the hybrid piston is more efficient with higher oxygen concentrations. Focusing on the main injection, it can be seen that the corresponding peak is also higher for the hybrid piston. This could be related with the better air-fuel mixing, which impacts in higher heat released by the main injection. In addition, the RoHR peak for the post injection is lower for the hybrid piston, indicating less residual of non-burned fuel during

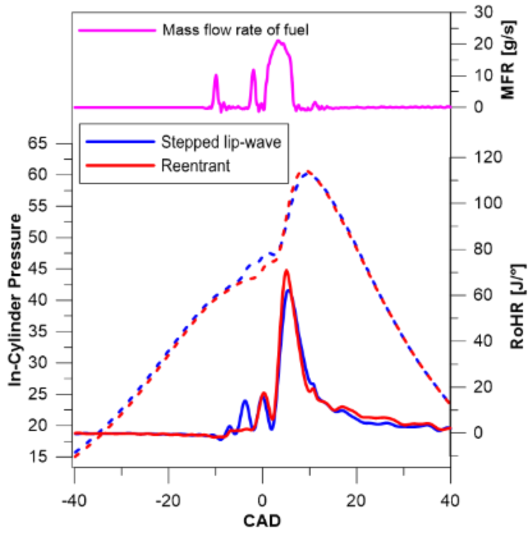

Figure 9- 4.5 bar IMEP – Reference case

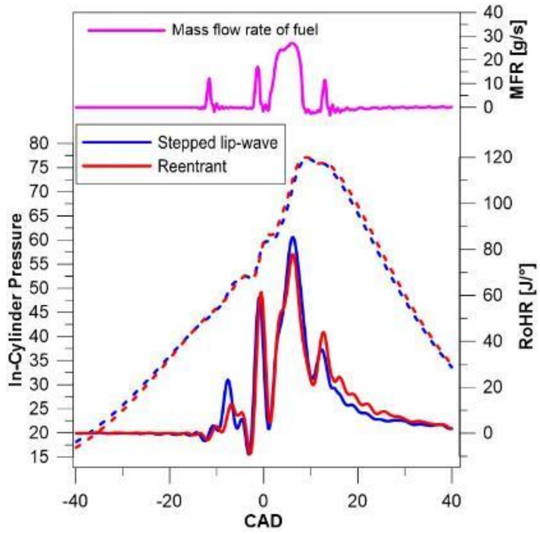

Figure 10- 8.9 bar IMEP (Similar OEM calibration)

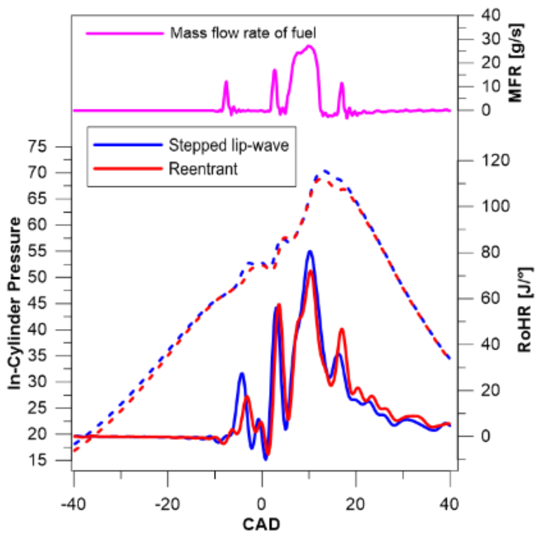

Figure 11- 8.9 bar IMEP +4 CAD

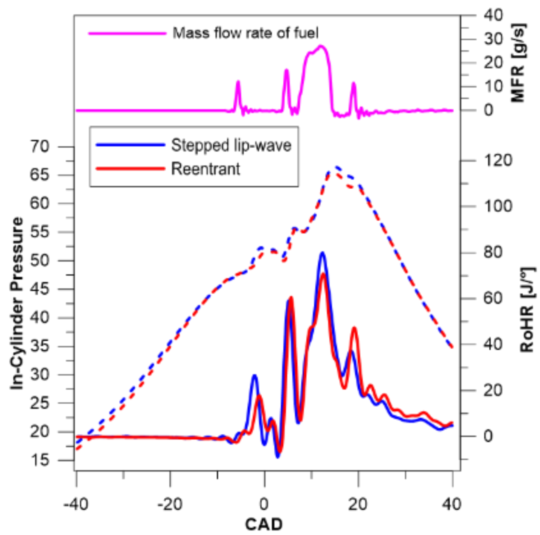

Figure 12-8.9 bar IMEP +6 CAD

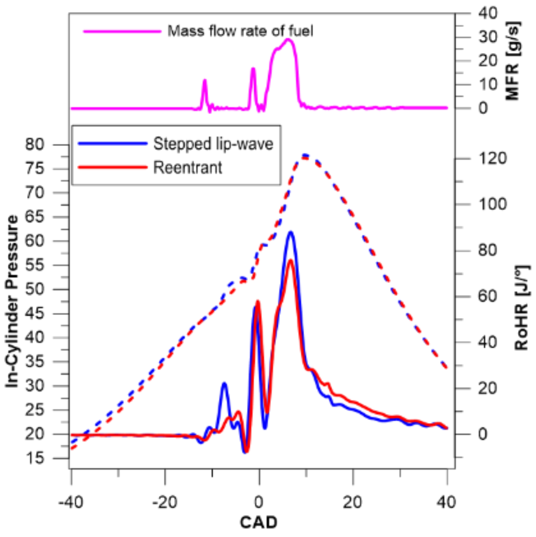

Figure 13- 8.9 bar IMEP- w/o post injection

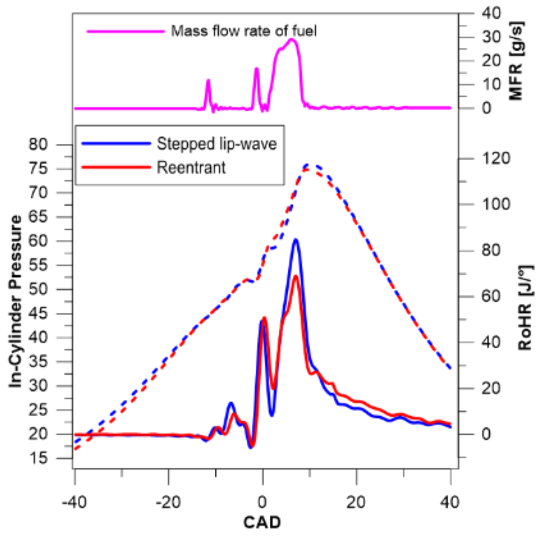

Figure 14- 8.9 bar IMEP- EGR-18% O_2 w/o post injection

the main injection combustion. Finally, at the end of the combustion process, it is possible to see that the RoHR of the hybrid piston decreases faster than for the reentrant one. This difference is more pronounced in cases without post injection (Figure 13 and Figure 14). In these cases, where late oxidation is not accelerated, the higher effectivity of the hybrid piston to produce late fuel and soot oxidation is visible.

In Figure 15 measurements of soot KL and OH* chemiluminescence for 4.5 bar IMEP are shown. In general, results show that the soot formation is higher for the re-entrant piston. The high soot concentration on the periphery of the re-entrant bowl is linked with the high momentum induced by the spray injection. The spray reaches the lip and, after that, most of the fuel is directed toward the center and spreads tangentially, promoting strong flame-flame interaction. This leads to the creation of fuel rich zones, which are key factor in the soot formation process. In contrast, with the hybrid piston, the sprays collide with the stepped lip and are split into two parts. One part of the fuel is sent to the squish region and the rest to the bowl [11]. This allows better air utilization and, as a consequence, reduces the soot pockets present in the late cycle oxidation.

The OH* signal is an indicator of the high temperature oxidation reactions and its intensity provides qualitative information about the OH* concentration. In general, the radiation registered for both pistons is similar. However, some differences can be observed. The first one appears at 11.71 CAD. At this instant, the reentrant piston shows OH* signal only at the center of the bowl and almost nothing at the periphery. However, the hybrid piston presents OH* chemiluminescence all around. As the RoHR shows (Figure 9), there is still heat release at this stage. Besides, at 16.21 CAD signal is visible again. Therefore, the lack of signal for the reentrant piston cannot be explained by a lack of oxidation. In fact, it has been related with the soot content. The higher soot formation for the reentrant piston causes OH* signal attenuation within the bowl[42]. It is possible to see a correspondence between low chemiluminescence and high soot KL. For the hybrid piston, soot levels are lower and OH* signal attenuation is not so severe.

At the end of the cycle (38.34 CAD) a more intense OH* chemiluminescence is observed for the reentrant piston. As soot KL at this stage is much lower or even negligible, no radiation absorption is taking place. Therefore, this difference proves that oxidation reactions are taking place later in the cycle than for the hybrid piston. This is coherent with the differences observed in terms of RoHR. In addition, the KL image shows for the re-entrant piston a soot area that has not yet finished to oxidize, which confirms that late oxidation is slower than for the hybrid piston.

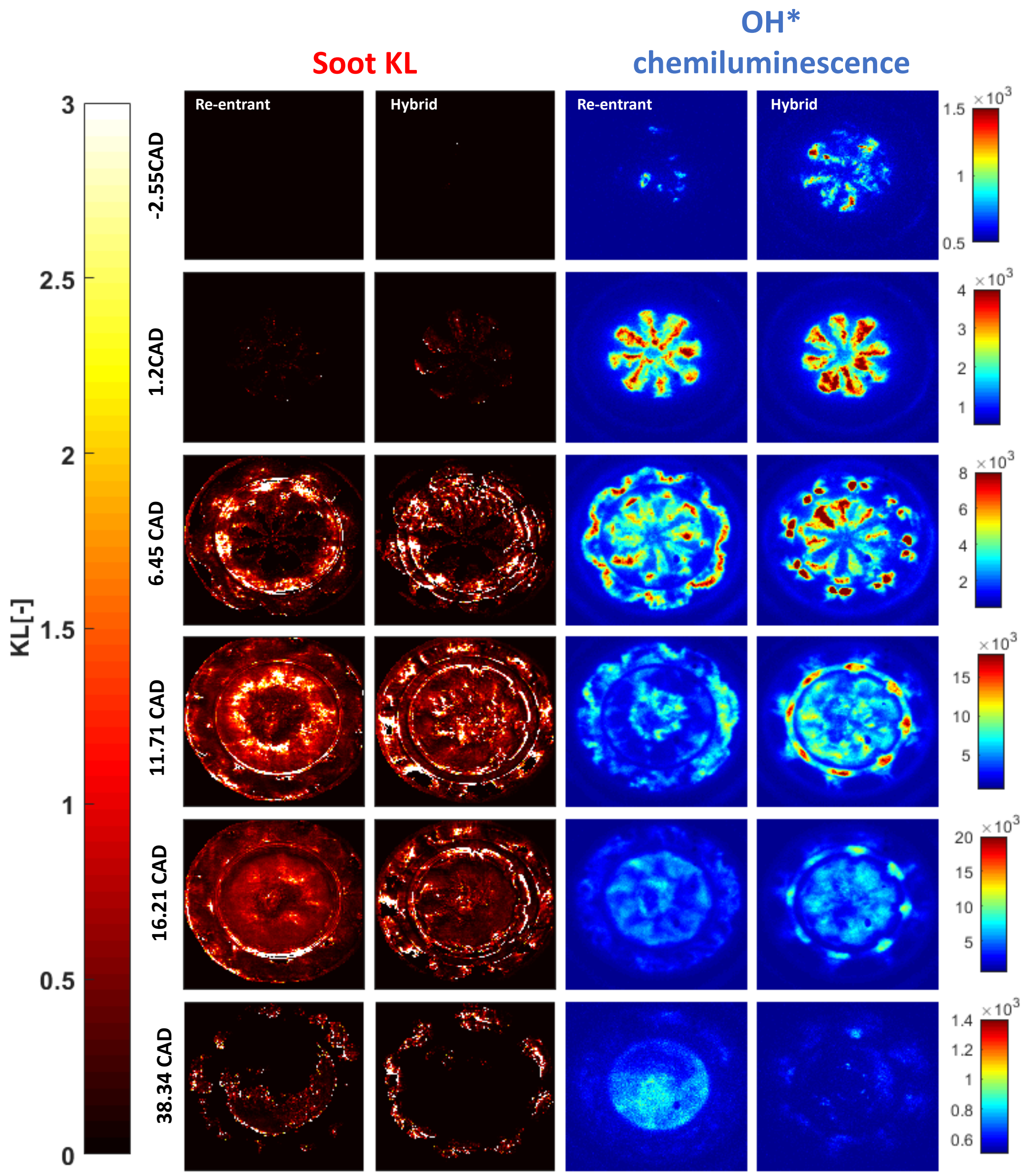

*Figure 15- KL and OH*chemiluminescence images at 4.5 bar IMEP*

The temporal evolution of the average KL and the accumulated flame radiation intensity registered by one of the high-speed cameras, at 4.5 bar IMEP is shown in Figure 16. In this Figure, hybrid piston KL has been split the two geometries and the average calculations were performed by using the same bowl regions shown previously in the methodology section in Figure 8. The same bowl region extension was considered for the re-entrant piston calculation. The curves show significantly higher soot formation for the re-entrant geometry. Besides, the oxidation phase is also slower than for any of the geometries of the hybrid piston, mainly during the late cycle burn-out phase (grey area). These results corroborate with the RoHR curve shown previously. Looking for the accumulated intensity behavior, the slower oxidation process for the re-entrant piston can be seen even more clearly as the reentrant piston shows a less steep curve. In addition, for this piston there is a delay between the maximum KL and the maximum intensity, which is caused by the soot self-attenuation. This is characteristic of high soot concentrations [37]. When comparing the stepped lip and stepped lip-wave, the peak KL values are similar. A different trend can be noted during the late cycle oxidation. In this case, the side with wave protrusions seems to oxidize faster than the side without lips.

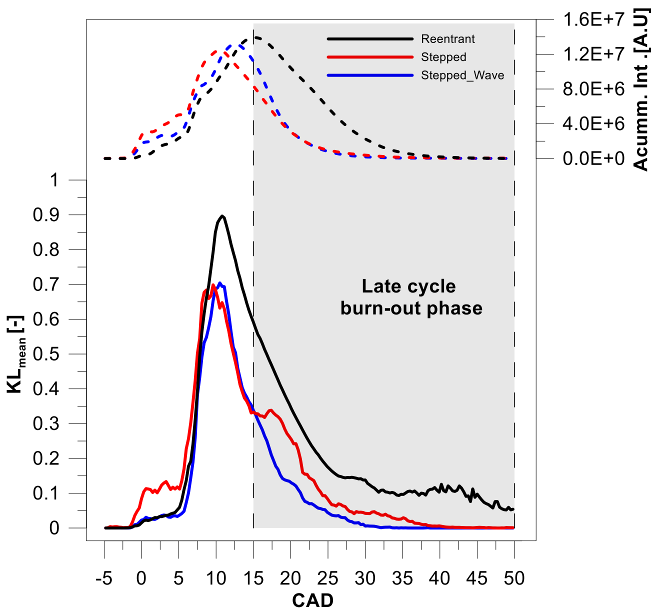

Figure 16-Mean KL and accumulated intensity at 4.5 bar IMEP

The Figure *17* presents the spatial and temporal evolution of the soot KL. These 2D evolution maps have been built by dividing each soot KL image in concentric ring areas, as described in the methodology section. The red discontinuous line is indicating the instant when the main injection energizing starts. The black line indicates the start of post injection energizing. For the re-entrant piston, the soot formation starts from the bowl periphery and goes toward the piston center. The KL reduction occurs smoothly, indicating a slower soot oxidation process. In addition, the areas with high soot concentration are much bigger than for the other two bowl geometries. As already explained previously, the re-entrant piston induces strong flame-flame interaction, promoting high soot formation during the first combustion stages. Thanks to the bowl geometry, which drives the flame toward the center and intensify the swirl movement, the formed soot can be oxidized, even if slowly. The reduction of soot formation for the hybrid piston can be seen clearly in the maps. In addition, for both stepped lip and stepped lip-wave side, the transitions of the colors are very abrupt, which indicate faster soot oxidation. This could be linked with the stepped lip effect as this feature is present at both sides of the hybrid piston. In contrast, the differences between stepped lip and stepped lip-wave geometries are less evident than when comparing with the re-entrant piston. The stepped lip bowl promotes a fast oxidation during the first stages of the combustion and most part of the soot is oxidized efficiently. However, as the combustion process evolves, the oxidation rate seems to decrease. From around 12 CAD to 20 CAD, a soot cloud remains inside the stepped lip bowl during some CADs until be completely oxidized. In contrast, for the stepped lip-wave, the soot is oxidized more efficiently during late cycle burn out phase, with a faster transition from the high values of KL to the low values, as shown previously in the KL means curves.

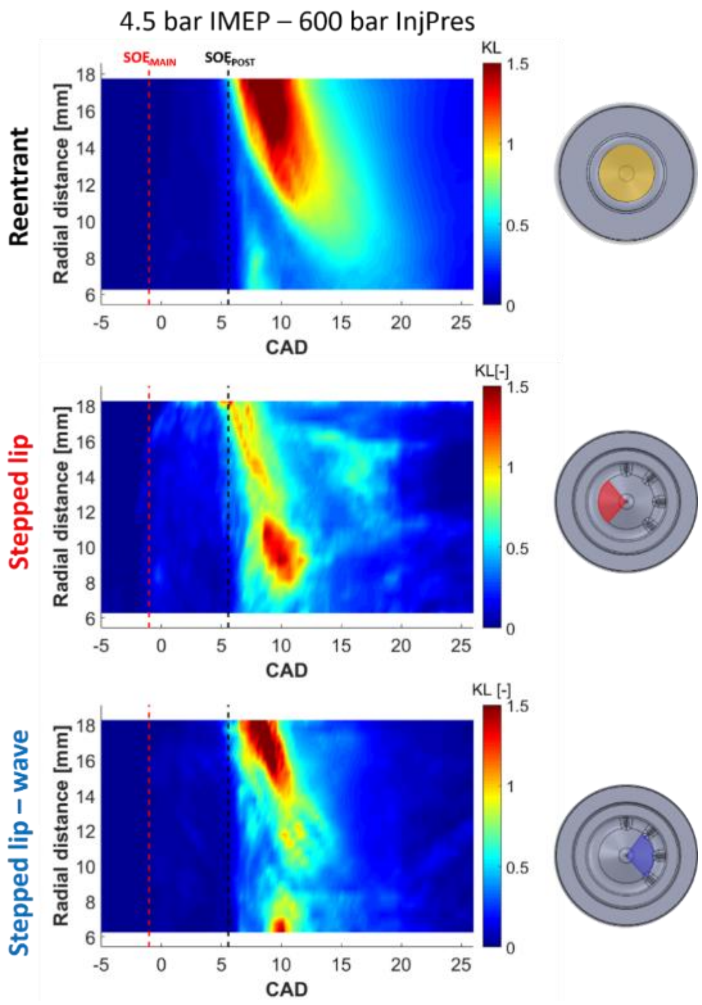

Figure 17 – 2D evolution mapa of KL at 4.5 bar IMEP

3.2. Stepped lip vs Stepped lip-wave

The benefits of the hybrid piston in comparison to the reentrant one have been demonstrated in the previous section. Besides, it has been possible to identify certain differences between the stepped lip and the stepped lip-wave geometries. In the following paragraphs, a deeper analysis of both geometries is performed in a variety of operating conditions where the soot formation is intensified.

Sweep of injection pulse train

In order to promote higher soot formation than the reference case and verify the potential of the waves in the soot oxidation process, the engine load was increased to 8.9 bar IMEP and injection pulses were delayed 4 and 6 CAD in relation to the case at 8.9 bar IMEP with similar OEM calibration. The increase of IMEP had the objective to increase the soot formation. In addition, by delaying the fuel injection, in-cylinder pressure and temperature are reduced and consequently, also the mixture reactivity. The temporal evolution of the average KL and accumulated flame radiation intensity for both geometries are shown in Figures 18, 19 and 20, respectively. The maximum soot KL seems to be very similar for both sides of the hybrid piston. In contrast, during the oxidation phase, the stepped lip-wave side is clearly promoting a faster soot oxidation, as it presents a steeper reduction. For the case without pulse delay (Figure 18), this effect is not so evident. In contrast, when the injection is delayed, the effect of the waves is more pronounced. The same behavior can be appreciated in the accumulated intensity curves.

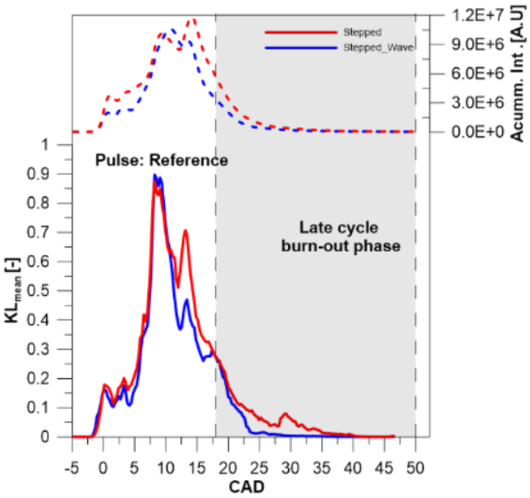

Figure 18- mean KL and accumulated intensity for reference pulse at 8.9 bar IMEP

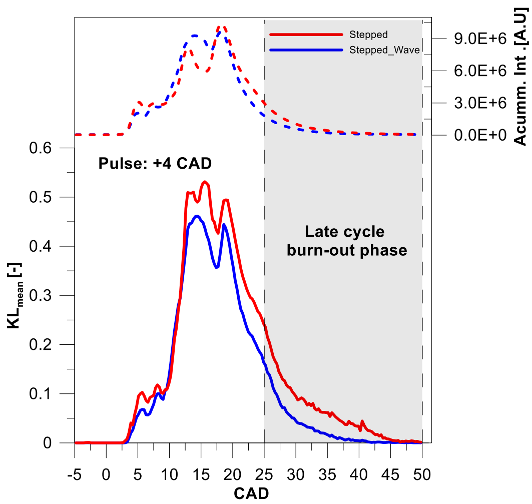

Figure 19- mean KL and accumulated intensity for 4 CAD of pulse delay at 8.9 bar IMEP

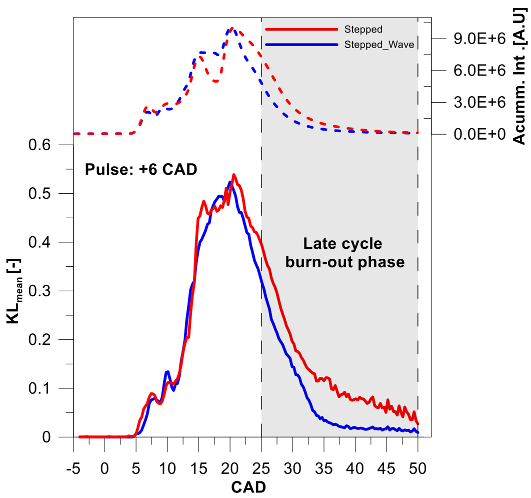

Figure 20- mean KL and accumulated intensity for 6 CAD of pulse delay at 8.9 bar IMEP

The Figure 21 shows soot KL evolution after the post injection have finished for the cases where the start of injection was delayed +4 and +6 CAD. In general, it is possible to see that the soot inside the bowl is slightly higher for the stepped lip side (left). In addition, the images show that the oxidation for the side without waves is slower. At 29.7 CAD, still a big soot area remains at the stepped lip side while much less soot is visible at the wave side (right).

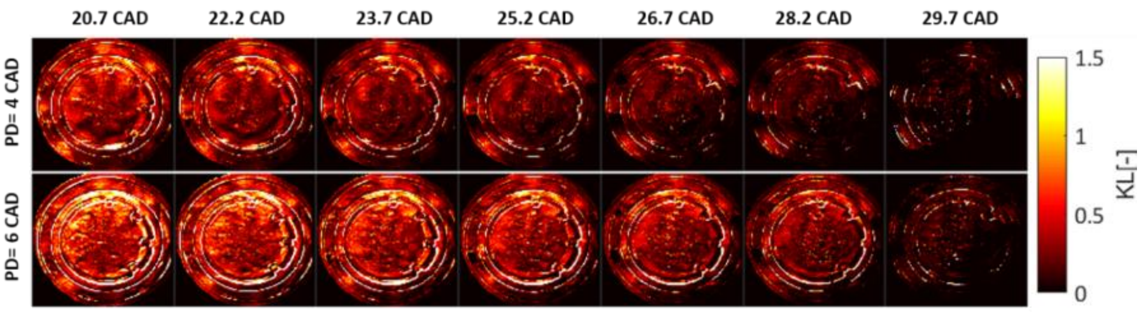

Figure 21- KL images at 8.9 bar IMEP for 4 CAD and 6 CAD pulse delay

The corresponding spatial and temporal evolution of soot KL for both sides of the hybrid piston is shown in Figure 22. They confirm the faster soot oxidation for the stepped lip-wave, as the KL values decrease faster along the corresponding part of the bowl. Besides, it can be highlighted, mainly for the injection delay cases that the stepped lip-wave side presents at first higher soot levels located at the bowl periphery. This could be related with the moment when the flame interacts with the waves and wall (cold surfaces), increasing momentarily the soot formation. However, the effect of redirecting the flame toward the center provides a rapid oxidation of this soot. As the flame is closer to the center, the KL value is lower. For the other side, without waves, the behavior is different. The soot seems to be uniformly distributed inside the combustion chamber, with higher values from the periphery to the bowl center. Thus, in this application the wave influence corroborates with previous results reported by Eismark et al.[12]. These authors reported that the waves induce a change in the flame shape, which generates better oxygen supply for all flame regions. The same behavior can be seen for both conditions tested.

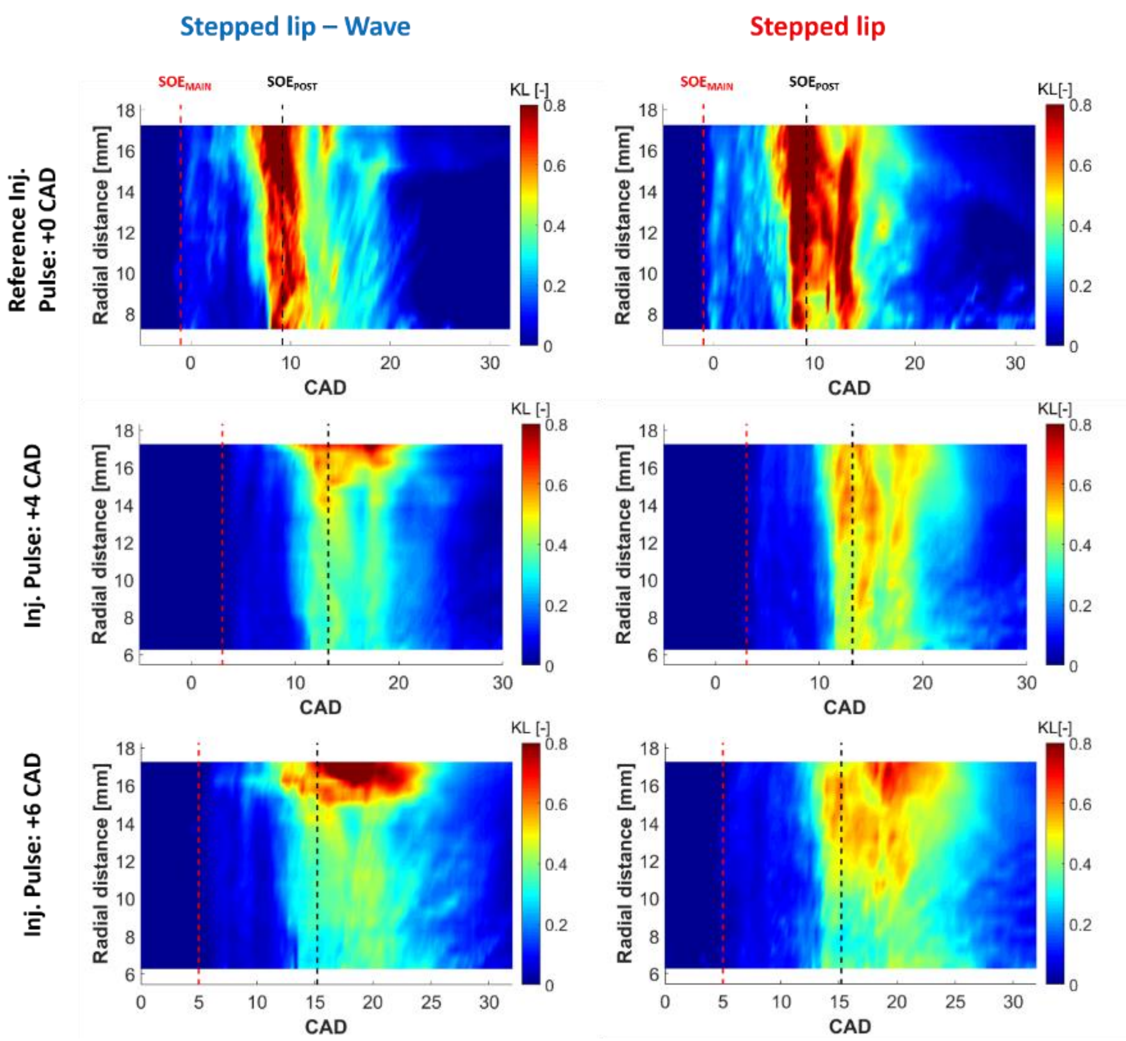

Figure 22- 2D evolution maps for SOE sweeps at 8.9 bar IMEP.

EGR effects

All the operating conditions previously analyzed include the use of post injection. It is widely known that it improves the soot oxidation at the late stages of combustion. Besides, most of the commercial compression ignition engines use EGR. The main objective of this technology is to reduce the NO_x formation, but it increases soot formation. In this way, high sooting conditions were also reproduced by removing the post injection and using EGR. In Figures 23 and 24, the evolution of accumulated flame intensity and average KL are shown for 8.9 IMEP, with and without EGR respectively. In both cases, no post injection was used. Under these conditions, the stepped lip-wave side continued showing the same characteristics reported when the post injection is used. Both piston sides, with and without waves, present similar maximum KL peak during the diffusion combustion phase, when the main injection is still occurring. However, clear differences can be appreciated during the late cycle oxidation, with significant faster oxidation for the stepped lip-wave side. In addition, at low oxygen concentration (EGR), the stepped lip side showed a higher difficulty to promote the oxidation of soot formed during the first combustion phase. In both cases, when the injection event ends and the KL values start to decrease, the stepped lip KL curves seems to change its slope, reducing the rate of soot oxidation.

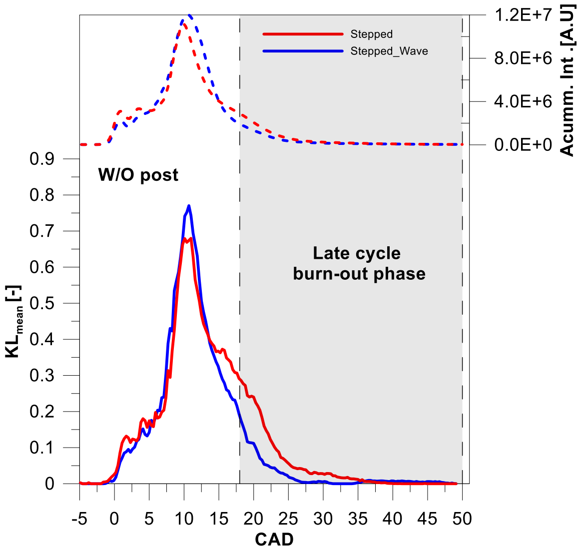

Figure 23- mean KL and accumulated intensity for the case w/o post injection

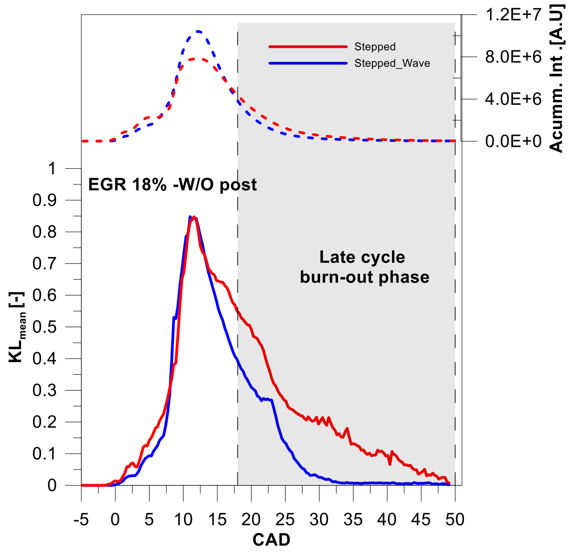

Figure 24- mean KL and accumulated intensity for the case with EGR and w/o post injection

The Figure 25 shows the KL spatial distribution for both conditions (with and without EGR) after the main injection ends. The benefits of the wave protrusions are visible, even under high soot conditions. For both cases, the stepped lip-wave (right bowl side) always presents less area covered by soot than the side without waves (left bowl side). What is more, it is possible to state that differences between both geometries are bigger when the oxygen concentration is reduced using EGR.

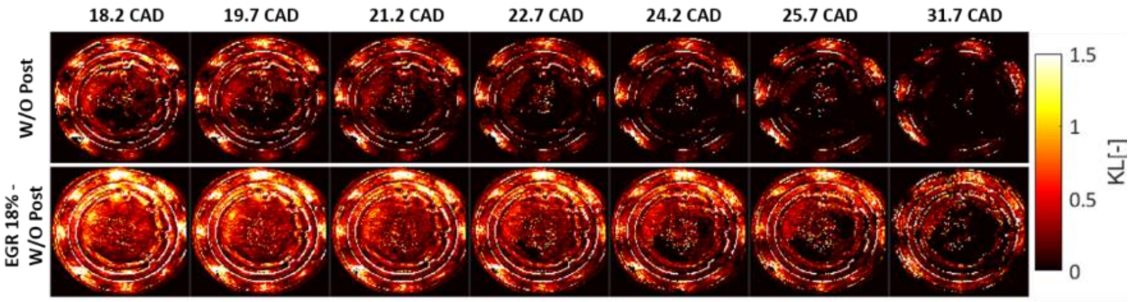

Figure 25- KL images at 8.9 bar IMEP for the case w/o post injection and for the case with EGR

4. Conclusions

An analysis of soot formation and oxidation of three different piston bowl geometries (re-entrant, stepped lip and stepped lip-wave) was performed by using an optical diesel engine. Two optical techniques, 2C pyrometry and OH* chemiluminescence, were applied to analyze the effect of the bowl geometries proposed on soot formation. The main results of the work are summarized below:

- The RoHR shows that, for all conditions tested, combustion process finishes earlier for the hybrid piston than for the re-entrant one. At the last part of the combustion, where the RoHR decreases, differences among pistons are visible. The hybrid piston seems to accelerate the process in comparison to the reentrant piston.
- The OH* signal extinguishes earlier for the hybrid piston, which confirms its shorter combustion duration.

- The reference case highlights the differences in terms of soot formation between the re-entrant and hybrid piston. A significant soot reduction, as well as a faster soot oxidation could be appreciated for the stepped lips and stepped lip-wave geometries in comparison with the re-entrant bowl.
- The sweep of SOE and EGR potentiated the effect of the waves. The mean KL and accumulated intensity curves always showed a faster soot oxidation for the stepped lip-wave side. In addition, the 2D evolution maps show that the wave protrusions initially produce more soot. However, they promote a faster soot oxidation. Without regard to the region close to the bowl wall, the wave side presents lower KL values than the other side of the piston.
- At the final stages of combustion, the steppe lip-wave side always presents less area covered by soot than the side without waves.

Acknowledgments

The authors gratefully acknowledge General Motors Propulsion Systems-Torino S.r.I. for support the project. Daniel Lérida for his laboratory work on the engine maintenance, operation, and control. This work was partially funded by Generalitat Valenciana through the Programa Santiago Grisolía (GRISOLIAP/2018/142) program.

References

1. Reitz RD, Ogawa H, Payri R, et al. IJER editorial: The future of the internal combustion engine. *Int J Engine Res* 2019; 21: 3–10.
2. Boggio SDM, Lacava PT, Merola S, et al. ScienceDirect Characterization of flame front propagation during early and late combustion for methane-hydrogen fueling of an optically accessible SI engine. *Int J Hydrogen Energy*; 3. Epub ahead of print 2018. DOI: 10.1016/j.ijhydene.2018.10.167.
3. Dallmann T, Posada F, Bandivadekar A. Costs of Emission Reduction Technologies for Diesel Engines Used in Non-Road Vehicles and Equipment. *Int Counc CLEAN Transp* 2018; 1–26.

4. Kozina A, Radica G, Ni S. Analysis of methods towards reduction of harmful pollutants from diesel engines. *J Clean Prod*; 262. Epub ahead of print 2020. DOI: 10.1016/j.jclepro.2020.121105.

5. Jiao Y, Liu R, Zhang Z, et al. Comparison of combustion and emission characteristics of a diesel engine fueled with diesel and methanol-Fischer-Tropsch diesel-biodiesel-diesel blends at various altitudes. *Fuel* 2019; 243: 52–59.

6. Lapuerta M, Ramos Á, Rubio S, et al. Optimization of a diesel engine calibration for operating with a residual glycerol-derived biofuel. *Int J Engine Res*. Epub ahead of print 2019. DOI: 10.1177/1468087419891535.

7. Karthic S V, Kumar MS, Nataraj G, et al. An assessment on injection pressure and timing to reduce emissions on diesel engine powered by renewable fuel. *J Clean Prod* 2020; 255: 120186.

8. Singh AP, Agarwal AK. Performance and emission characteristics of conventional diesel combustion/partially premixed charge compression ignition combustion mode switching of biodiesel-fueled engine. *Int J Engine Res*. Epub ahead of print 2019. DOI: 10.1177/1468087419860311.

9. Uchida N, Watanabe H. A new concept of actively controlled rate of diesel combustion (ACCORDIC): Part II—simultaneous improvements in brake thermal efficiency and heat loss with modified nozzles. *Int J Engine Res* 2019; 20: 34–45.

10. Hua Y, Liu F, Wu H, et al. Effects of alcohol addition to traditional fuels on soot formation: A review. *Int J Engine Res* 2020; 1468087420910886.

11. Busch S, Zha K, Perini F, et al. Bowl Geometry Effects on Turbulent Flow Structure in a Direct Injection Diesel Engine. *SAE Tech Pap*; 2018-Septe. Epub ahead of print 2018. DOI: 10.4271/2018-01-1794.

12. Eismark J, Christensen M, Andersson M, et al. Role of fuel properties and piston shape in influencing soot oxidation in heavy-duty low swirl diesel engine combustion. *Fuel* 2019; 254: 115568.

13. Li B, Liu H, Yu L, et al. Optimization of piston bowl and valve system in compression ignition engine fueled with gasoline/diesel/polyoxymethylene dimethyl ethers for high efficiency. *Int J Engine Res*. Epub ahead of print 2019. DOI: 10.1177/1468087419865384.

14. Leach F, Ismail R, Davy M, et al. The effect of a stepped lip piston design on performance and emissions from a high-speed diesel engine. *Appl Energy* 2018; 215: 679–689.

15. Shrivastava P, Verma TN. Effect of fuel injection pressure on the characteristics of CI engine fuelled with biodiesel from Roselle oil. *Fuel* 2020; 265: 117005.

16. Agarwal AK, Srivastava DK, Dhar A, et al. Effect of fuel injection timing and pressure on combustion, emissions and performance characteristics of a single cylinder diesel engine. *Fuel* 2013; 111: 374–383.

17. Molina S, García A, Monsalve-Serrano J, et al. Effects of fuel injection parameters on premixed charge compression ignition combustion and emission characteristics in a medium-duty compression ignition diesel engine. *Int J Engine Res*. Epub ahead of print 2019. DOI: 10.1177/1468087419867014.

18. Kumar S, Dinesha P, Rosen MA. Effect of injection pressure on the combustion, performance and emission characteristics of a biodiesel engine with cerium oxide nanoparticle additive. *Energy* 2019; 185: 1163–1173.

19. Gumus M, Sayin C, Canakci M. The impact of fuel injection pressure on the exhaust emissions of a direct injection diesel engine fueled with biodiesel-diesel fuel blends. *Fuel* 2012; 95: 486–494.

20. Zha K, Busch S, Warey A, et al. A Study of Piston Geometry Effects on Late-Stage Combustion in a Light-Duty Optical Diesel Engine Using Combustion Image Velocimetry. *SAE Int J Engines* 2018; 11: 783–804.

21. Rao L, Zhang Y, Kim D, et al. Effect of after injections on late cycle soot oxidation in a small-bore diesel engine. *Combust Flame* 2018; 191: 513–526.

22. Genzale CL, Reitz RD, Musculus MPB. Effects of piston bowl geometry on mixture development and late-injection low-temperature combustion in a heavy-duty diesel engine. *SAE Int J Engines* 2009; 1: 913–937.

23. Benajes J, Pastor J V., García A, et al. An experimental investigation on the influence of piston bowl geometry on RCCI performance and emissions in a heavy-duty engine. *Energy Convers Manag* 2015; 103: 1019–1030.

24. Eismark J, Balthasar M, Karlsson A, et al. Role of late soot oxidation for low emission combustion in a diffusion-controlled, High-EGR, heavy duty diesel engine. *SAE Tech Pap* 2009; 4970: 1–15.

25. Pastor M, Monsalve-serrano J, Benajes J, et al. Effects of piston bowl geometry on Reactivity Controlled Compression Ignition heat transfer and combustion losses at different engine loads. 2016; 98: 64–77.

26. Dahlstrom J, Andersson O, Tuner M, et al. Experimental Comparison of Heat Losses in Stepped-Bowl and Re-Entrant Combustion Chambers in a Light Duty Diesel Engine. *SAE Tech Pap*. Epub ahead of print 2016. DOI: 10.4271/2016-01-0732.

27. Busch S, Perini F. Progress toward understanding vortex generation in stepped-lip diesel engine combustion chambers. *Results Eng* 2019; 1: 100004.

28. Yoo D, Kim D, Jung W, et al. Optimization of diesel combustion system for reducing PM to meet tier4-final emission regulation without diesel particulate filter. *SAE Tech Pap*; 11. Epub ahead of print 2013. DOI: 10.4271/2013-01-2538.

29. Neely GD, Sasaki S, Sono H. Investigation of Alternative Combustion Crossing Stoichiometric Air Fuel Ratio for Clean Diesels. Epub ahead of print 2007. DOI: https://doi.org/10.4271/2007-01-1840.

30. Smith A. Ricardo low emissions combustion technology helps JCB create the off-

highway industry ’ s cleanest engine. *Ricardo Press Release* 2010; 4–6.

31. Cornwell R, Conicella F. *DIRECT INJECTION DIESEL ENGINES*. US Patent 8,770,168 B2, 2011.

32. Yoo D, Kim D, Jung W, et al. Optimization of Diesel Combustion System for Reducing PM to Meet Tier4-Final Emission Regulation without Diesel Particulate Filter. Epub ahead of print 2013. DOI: https://doi.org/10.4271/2013-01-2538.

33. Eder T, Kemmner M, Lückert P, et al. OM 654 – Launch of a New Engine Family by Mercedes-Benz. 2016; 18–25.

34. Eismark J, Andersson M, Christensen M, et al. Role of Piston Bowl Shape to Enhance Late-Cycle Soot Oxidation in Low-Swirl Diesel Combustion. *SAE Int J Engines*; 12. Epub ahead of print 25 April 2019. DOI: 10.4271/03-12-03-0017.

35. Zhang T, Eismark J, Munch K, et al. Effects of a wave-shaped piston bowl geometry on the performance of heavy duty Diesel engines fueled with alcohols and biodiesel blends. *Renew Energy* 2020; 148: 512–522.

36. Zhao H. *Laser Diagnostics and Optical Measurement Techniques in Internal Combustion Engines*. SAE International, 2012.

37. Pastor J V., García A, Micó C, et al. Application of optical diagnostics to the quantification of soot in n -alkane flames under diesel conditions. *Combust Flame* 2015; 164: 212–223.

38. Xuan T, Pastor J V., García-Oliver JM, et al. In-flame soot quantification of diesel sprays under sooting/non-sooting critical conditions in an optical engine. *Appl Therm Eng* 2019; 149: 1–10.

39. Payri F, Molina S, Martín J, et al. Influence of measurement errors and estimated parameters on combustion diagnosis. *Appl Therm Eng* 2006; 26: 226–236.

40. Payri F, Olmeda P, Martín J, et al. A complete 0D thermodynamic predictive model for direct injection diesel engines. *Appl Energy* 2011; 88: 4632–4641.

41. Pastor J, Olmeda P, Martín J, et al. Methodology for Optical Engine Characterization by Means of the Combination of Experimental and Modeling Techniques. *Appl Sci* 2018; 8: 2571.

42. Rochussen J, McTaggart-Cowan G, Kirchen P. Parametric study of pilot-ignited direct-injection natural gas combustion in an optically accessible heavy-duty engine. *Int J Engine Res* 2019; 21: 497–513.

Nomenclature

2C – Two color pyrometry

CAD- Crank angle degree

CI- Compression Ignition

C_r- Compression Ratio

EGR- Exhaust Gas Recirculation

FPS- Frames per second

ICE - Internal combustion engines

IMEP- Indicated mean effective pressure

MFR- Mass flow rate

NL- Natural Luminosity

NO_X- Nitrogen dioxide and monoxide

OEM- Original Equipment Manufacturer

Pinj – Injection pressure

Pint – Intake pressure

P_{max}- Maximum in-cylinder pressure

RoHR- Rate of heat release

rpm – engine speed

SOE- Start of energizing

FWHM – Full width at half maximum

Tcool – Coolant temperature

Tint – Intake temperature

Toil – Oil temperature

ULPC - Ultra-Low Particulate Combustion

UV – Ultraviolet